

## Electron-Paramagnetic-Resonance and Optical Spectra of $\text{Cr}^{3+}$ in $\text{SnO}_2$ Single Crystals

S. L. HOU, R. W. SUMMITT,\* AND R. F. TUCKER

Corning Glass Works Research Laboratory, Corning, New York

(Received 15 August 1966)

EPR and optical spectra have been obtained for  $\text{Cr}^{3+}$ -doped  $\text{SnO}_2$  crystals both as grown and after subsequent heat treatment. Two distinct EPR and optical spectra have been observed.  $(\text{EPR})_I$  and  $(\text{Opt})_I$  are characteristic of the as-grown crystal. The  $(\text{EPR})_I$  is shown to be due to  $\text{Cr}^{3+}$  in substitutional sites with spin Hamiltonian parameters  $D = -0.6840 \pm 0.0002 \text{ cm}^{-1}$ ,  $E = 0.1852 \pm 0.0002 \text{ cm}^{-1}$ , and  $g_{av} = 1.975$ . The lines are superhyperfine-broadened with superhyperfine structure (shfs) of two- and four-tin nuclei approximately equal to 35 and 7 G, respectively. EPR spectra of  $\text{Fe}^{3+}$  and  $\text{V}^{4+}$  show some similarities in shfs. The  $(\text{Opt})_I$  spectrum consists of intense bands centered at  $18\,250 \text{ cm}^{-1}$  and  $19\,400 \text{ cm}^{-1}$  ( $\alpha \sim 100 \text{ cm}^{-1}$ ,  $\Delta\nu \sim 3000 \text{ cm}^{-1}$ ) with light polarized perpendicular and parallel to the  $c$  axis, respectively. After heating in a reducing atmosphere,  $(\text{Opt})_I$  disappears completely. New weak bands  $(\text{Opt})_{II}$  appear at slightly different energies of  $21\,400 \text{ cm}^{-1}$  and  $19\,700 \text{ cm}^{-1}$  ( $\alpha \sim 0.6 \text{ cm}^{-1}$ ,  $\Delta\nu \sim 800 \text{ cm}^{-1}$ ) with light polarized perpendicular and parallel to the  $c$  axis, respectively. The EPR measurements of the reduced crystal shows that: (1) 75% of the  $\text{Cr}^{3+}$  ions are still in the substitutional site; (2) a new spectrum  $(\text{EPR})_{II}$  with four nonequivalent sites is observed with spin Hamiltonian parameters  $D = -0.7033 \pm 0.0002 \text{ cm}^{-1}$ ,  $E = 0.1448 \pm 0.0002 \text{ cm}^{-1}$ , and  $g_{av} = 1.975$ . The shfs for two and four tin nuclei are approximately 38 and 9 G, respectively.  $(\text{EPR})_{II}$  may be due to  $\text{Cr}^{3+}$  ions in interstitial positions. Reheating in  $\text{O}_2$  atmosphere restores the original spectra. Results correlate  $(\text{EPR})_I$  with  $(\text{Opt})_{II}$ . Hence  $10Dq \cong 20\,000 \text{ cm}^{-1}$  and the tetragonal distortion is about  $2000 \text{ cm}^{-1}$ .

### I. INTRODUCTION

SINGLE crystals of  $\text{SnO}_2$  doped with ( $3d$ ) transition metal ions have been grown from the vapor phase.<sup>1</sup> The  $\text{Cr}^{3+}$  concentration is about 250 ppm, while the concentrations of other impurities are down to a few parts per million. The electron-paramagnetic-resonance EPR and optical spectra have been measured both at room temperature and low temperatures. Heat treatments produced gross changes in both spectra, including an EPR spectrum possibly due to interstitial  $\text{Cr}^{3+}$ .

Section II indicates the symmetry of the angular dependence of EPR spectra in various sites. Section III describes the experimental setup. Section IV discusses the EPR spectrum of  $\text{Cr}^{3+}$  of an as-grown crystal and the relation between SHF interaction and the line shape. The optical spectrum and the EPR spectrum of  $\text{Cr}^{3+}$  resulting from various heat treatments are described in Sec. V and Sec. VI, respectively, and the final discussions and conclusions are given in Sec. VII.

### II. THE SYMMETRY AND CRYSTAL STRUCTURE OF $\text{SnO}_2$

$\text{SnO}_2$  crystalizes in the rutile structure<sup>1-3</sup> which is illustrated in Fig. 1. The unit cell, which has  $D_{4h}$  symmetry, contains two sites which have  $D_{2h}$  symmetry. Each tin ion is octahedrally surrounded by six oxygen ions at equal distances. However, if a  $3d$ -impurity ion substitutes for the tin ion, an axial distortion is intro-

duced because of a different ionic radius and a different charge (if any). Furthermore, the four oxygen ions in the  $(1\bar{1}0)$  plane are located in the corners not forming right angles with the tin ion ( $78.1^\circ$ ); hence a rhombic distortion exists. The symmetry axes of each site, namely the  $[110]$ ,  $[1\bar{1}0]$ , and  $c$  axes, are chosen as the principal axes. In particular, the  $[110]$  axis, which has two oxygen ions in the same  $c$  coordination as the tin ion, is chosen as the  $z$  axis, and the  $c$  axis is chosen as the  $x$  axis. The measured angular dependence verifies the choice of the principal axes.

Impurities are usually located substitutionally in a tin ion site. For substitutionally located impurities, there are two nonequivalent sites in a unit cell as shown in Fig. 2 where each arrow represents the tetragonal axis of the site. These two sites are magnetically equivalent when  $H_{dc} \parallel [100]$  (or  $[010]$ ). A similar

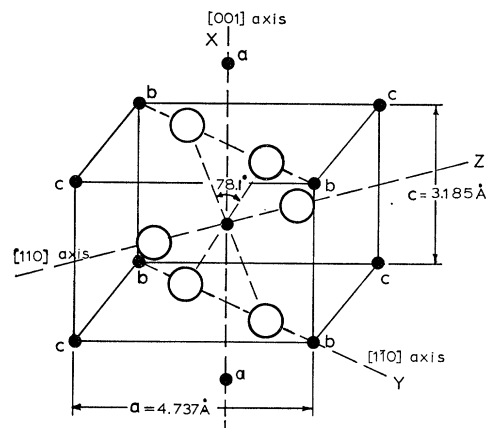


FIG. 1. Crystal structure of  $\text{SnO}_2$ . Filled in circles Sn atom; open circles O atom.

\* Present address: Department of Metallurgy, Mechanics and Material Science, Michigan State University, East Lansing, Michigan.

<sup>1</sup> J. A. Marley and T. C. MacAvoy, Corning Glass Works Project Report No. 5621, 1962 (unpublished).

<sup>2</sup> R. W. G. Wyckoff, *Crystal Structures* (Interscience Publishers, Inc., N. Y., 1953), Vol. III.

<sup>3</sup> Von Werner and H. Baur, *Acta Cryst.* **9**, 515 (1956).

situation occurs when  $H_{dc} \parallel c$  axis. Resonance lines are therefore expected to cross at the 100 axis and  $c$  axis.

There are two possible interstitial locations. The first possible locations are  $[\pm(a/2), 0, n(C/2)]$  and  $[0, \pm(a/2), n(C/2)]$ , where  $n$  is an integer. A paramagnetic ion in this location is octahedrally surrounded by six oxygen ions with their tetragonal axis tilted  $+13^\circ$  from the  $[110]$  axis and is also octahedrally surrounded by six tin ions with their tetragonal axis tilted  $-45^\circ$  from the  $[110]$  axis. The resultant magnetic  $z$  axis of the paramagnetic ion would be expected to tilt an angle  $\theta$  with respect to the  $[110]$  axis, where  $13^\circ > \theta > -45^\circ$ . The site symmetry is  $C_{2h}$  (one twofold axis along the  $c$  axis). There are 8 such sites in the unit cell equivalent in pairs giving 4 nonequivalent sites per unit cell. Two of them will be magnetically equivalent when  $H_{dc} \parallel [110]$  axis and  $H_{dc} \parallel [100]$  axis. All sites are magnetically equivalent if  $H_{dc} \parallel c$  axis. This is illustrated in Fig. 3. The second possible interstitial locations are  $[\pm(a/2), 0, \pm(c/4)]$  and  $[0, \pm(a/2), \pm(c/4)]$ , where each ion is in a tetrahedral environment. There are only two nonequivalent sites per unit cell. They are magnetically equivalent if  $H_{dc} \parallel [110]$  axis and  $H_{dc} \parallel c$  axis.

### III. THE EXPERIMENTAL SETUP

The EPR spectrum was measured using a Varian X-band spectrometer at 9.5 kMc. A crystal video detection at 100-kc modulation frequency was used at room temperature. A superheterodyne system was used at low temperatures (1.5 to 4.2°K). To avoid saturation due to a long spin-lattice relaxation time at low temperatures, the incident power was reduced to  $\sim 10^{-9}$  W. An external ac modulation field of 0.5 G (peak to peak) at 9.5 cps was also used. The dc magnetic field was provided by a Varian 12-in. magnet, swept at 1.0 G/min, and was measured by a proton gauss-meter with an accuracy of  $\pm 0.2$  G.

The optical spectra were recorded using Perkin-Elmer model 350 and Cary Model 14 spectrometers with light polarized by Polaroid type HNP'B sheet polarizers. Low-temperature (down to 20°K) data were obtained using a cryotip refrigerator and Dewar fitted with fused silica windows.

### IV. EPR OF $\text{Cr}^{3+}$ IN $\text{SnO}_2$ IN AN AS-GROWN CRYSTAL

#### 1. The Spin Hamiltonian

The spin Hamiltonian of a  $\text{Cr}^{3+}$  ion in a  $D_{2h}$  site symmetry with  $S = \frac{3}{2}$  is usually written as

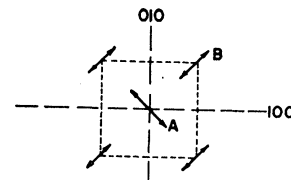
$$3\mathcal{C}_s = D[S_z^2 - \frac{1}{3}S(S+1)] + E[S_x^2 - S_y^2] + \beta \mathbf{H} \cdot \mathbf{g} \cdot \mathbf{S} + \mathbf{S} \cdot \mathbf{A}_{\text{Cr}} \cdot \mathbf{I}_{\text{Cr}} + \sum_{\text{Sn}} \mathbf{S} \cdot \mathbf{A}_{\text{Sn}} \cdot \mathbf{I}_{\text{Sn}}, \quad (1)$$

where the spin-Hamiltonian parameters  $D$ ,  $E$ , and  $g$  are related by the  $\Delta$ -tensor elements,<sup>4,5</sup>  $\mathbf{S} \cdot \mathbf{A}_{\text{Cr}} \cdot \mathbf{I}_{\text{Cr}}$  is

<sup>4</sup> M. H. L. Pryce, Proc. Roy. Soc. (London) **A214**, 237 (1952).

<sup>5</sup> S. L. Hou and N. Bloembergen, Phys. Rev. **138**, A1218 (1965).

FIG. 2. The schematic diagram of tetragonal axes of substitutional sites.



the hyperfine interaction for the  $\text{Cr}^{53}$  ion;  $\sum_{\text{Sn}} \mathbf{S} \cdot \mathbf{A}_{\text{Sn}} \cdot \mathbf{I}_{\text{Sn}}$  is the superhyperfine interaction between  $(3d)^3$  electrons and the nearest-neighbor  $\text{Sn}^{119}$  and  $\text{Sn}^{117}$  nuclei. The symmetry axes of the site are chosen as the principal axes as mentioned in Sec. II. The orbital angular momentum operator  $\mathbf{L}$  of the spin-orbit interaction, which transforms like  $T_1$  in the  $O_h$  group, connects the ground orbital state  ${}^4A_2$  to the excited orbital states  ${}^4T_2$  only. The isotropic part of the  $g$  tensor is obtained as  $2.0023 - (8\lambda/10Dq) = 1.975$ .

If we ignore the last two terms in Eq. (1), (or we set  $m_I = 0 = \sum_{\text{Sn}} m_I$ ), the energy eigenvalues can be solved exactly. The zero field splitting can be obtained as  $2(D^2 + 3E^2)^{1/2}$ , and the ratio of the  $|\mp \frac{3}{2}\rangle$  state mixing into the predominant  $|\pm \frac{1}{2}\rangle$  state, or vice versa, is  $R = 3E/[D \pm (D^2 + 3E^2)^{1/2}]$ .

If a dc magnetic field is applied along any one of the principal axes, the four energy levels can be obtained exactly. If  $H_{dc} \parallel z$  axis, we have

$$\begin{aligned} W_{1,3} &= +\frac{1}{2}g\beta H_z \pm [(D + g\beta H_z)^2 + 3E^2]^{1/2}, \\ W_{2,4} &= -\frac{1}{2}g\beta H_z \pm [(D - g\beta H_z)^2 + 3E^2]^{1/2}. \end{aligned} \quad (2)$$

If  $H_{dc} \parallel x$  axis, we have

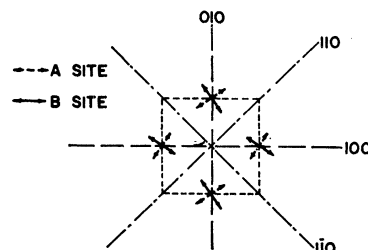
$$\begin{aligned} W_{1,3} &= \frac{1}{2}g\beta H_x \pm [(D - \frac{1}{2}g\beta H_x)^2 + 3(E + \frac{1}{2}g\beta H_x)^2]^{1/2}, \\ W_{2,4} &= -\frac{1}{2}g\beta H_x \pm [(D + \frac{1}{2}g\beta H_x)^2 + 3(E - \frac{1}{2}g\beta H_x)^2]^{1/2}. \end{aligned} \quad (3)$$

If  $H_{dc} \parallel y$  axis, we have

$$\begin{aligned} W_{1,3} &= \frac{1}{2}g\beta H_y \pm [(D - \frac{1}{2}g\beta H_y)^2 + 3(E - \frac{1}{2}g\beta H_y)^2]^{1/2}, \\ W_{2,4} &= -\frac{1}{2}g\beta H_y \pm [(D + \frac{1}{2}g\beta H_y)^2 + 3(E + \frac{1}{2}g\beta H_y)^2]^{1/2}. \end{aligned} \quad (4)$$

The angular dependence for the EPR spectrum of  $\text{Cr}^{3+}$  in the as-grown crystal is shown in Fig. 4. Lines from inequivalent sites cross when  $H_0$  is parallel to the  $[100]$  axis, and the  $c$  axis. According to the discussion given in Sec. II, all  $\text{Cr}^{3+}$  ions are in substitutional sites. There are transitions within predominantly  $\pm \frac{1}{2}$  and predominantly  $\pm \frac{3}{2}$  doublets and transitions such as  $|+\frac{3}{2}\rangle \leftrightarrow |\frac{1}{2}\rangle$  at fields  $H_{dc} > 9600$  G. The transition

FIG. 3. The schematic diagram of tetragonal axes of interstitial sites.



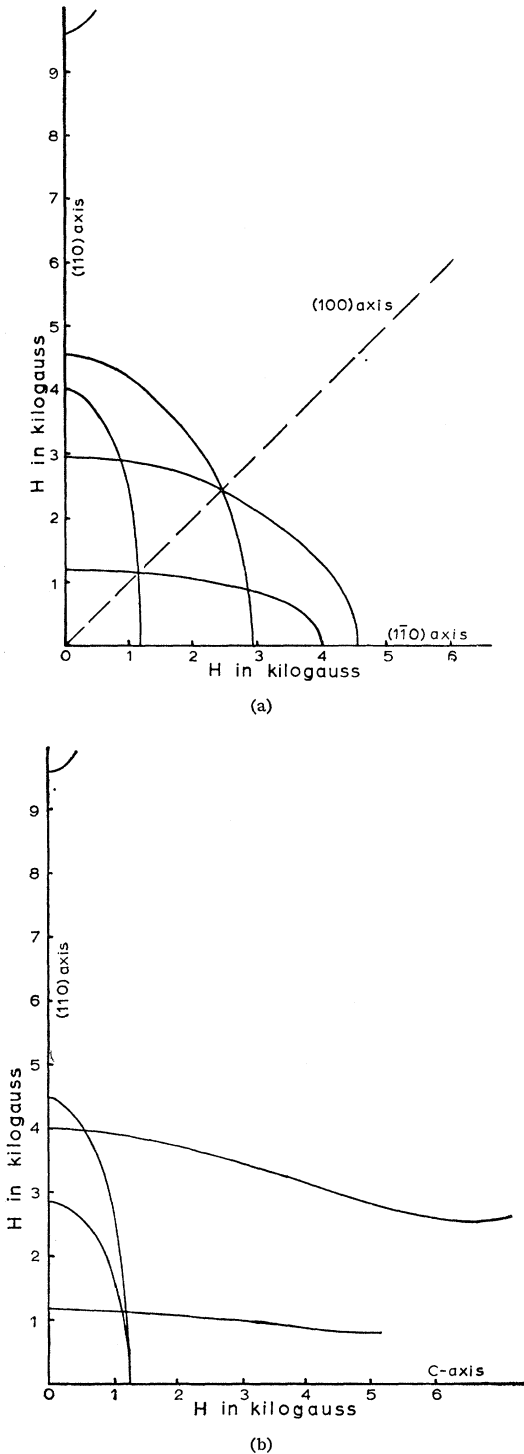


FIG. 4. The angular dependence of the EPR spectrum of an as-grown  $\text{Cr}^{3+}$ -doped  $\text{SnO}_2$  (a) on the  $c$  plane; and (b) on a plane containing the  $[110]$  axis and the  $c$  axis.

within the  $\pm\frac{3}{2}$  doublet is allowed because of the state mixing in the presence of rhombic distortion  $E(S_x^2 - S_y^2)$ . The intensity, however, is down to about

$\frac{1}{3}$  of that of the  $\pm\frac{1}{2}$  doublet transition. The major axes of the ellipses and the hyperbola in Fig. 4 verify the choice of principal axes described in Sec. II. Using Eqs. 2, 3, and 4, we get the parameters of the spin Hamiltonian as  $g_{av} = 1.975$ ,  $D = -0.6840 \pm 0.0002 \text{ cm}^{-1}$ ,  $E = 0.1851 \pm 0.0002 \text{ cm}^{-1}$ , and a zero-field splitting of  $1.5108 \text{ cm}^{-1}$ . From<sup>6</sup> measured the EPR spectrum of  $\text{Cr}^{3+}$  in  $\text{SnO}_2$ ; his sign of  $D$  differs from that which we obtain after a proper transformation of principal axes. The temperature dependence of the intensity ratio of  $\pm\frac{1}{2}$  and  $\pm\frac{3}{2}$  transitions indicates that  $D < 0$  as shown in Fig. 5. The energy levels versus the dc magnetic field are shown in Fig. 6.

## 2. Superhyperfine Interaction and Line Shapes

The hyperfine (hf) and the superhyperfine (shf) interactions are obtained from the interaction of the electron spin with the nuclear spin.<sup>7</sup> The dominant contribution to the hf (or shf) tensor arises from the exchange polarization of the core electrons by the spin density of the unpaired ( $3d$ ) electrons.<sup>8</sup>

By comparing the hf (or shf) interaction  $A_z S_z I_z$  with  $g\beta S_z H_z$ , the hf (or shf) interaction is equivalent to an effective magnetic field  $H_{\text{eff}} = A_z m_I / g\beta$  in the spin Hamiltonian. If  $|g\beta H| \gg |A_z|$ , the additional energy splittings due to hf (or shf) interaction can be expressed as  $(\partial W_i / \partial H) |_{H_0} (A_z m_I / g\beta) = m_I \Delta W_i$  to first order. The selection rule of allowed transitions is  $\Delta m_s = \pm 1$  and  $\Delta m_I = 0$ , since the transition matrix is of the form  $(S^+ h^- + S^- h^+)$  (where "h" is the rf magnetic field). Let  $W_i(H_0)$  and  $W_j(H_0)$  be two levels of an allowed transition with  $m_I = 0$ , i.e.,  $h\nu = W_i(H_0) - W_j(H_0)$ . Since the microwave frequency  $\nu$  is fixed, an extra magnetic field ( $\Delta H_0$ ) is required to observe the additional energy splittings due to hf (or shf) interaction at different  $m_I$ ,

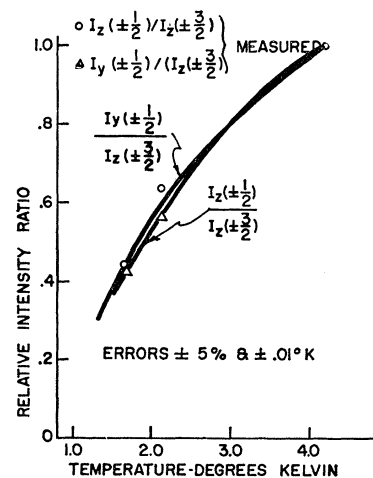


FIG. 5. The temperature dependence of intensity ratio of predominantly  $\pm\frac{1}{2}$  and  $\pm\frac{3}{2}$  transitions.

<sup>6</sup> W. H. From, Phys. Rev. **131**, 961 (1963).

<sup>7</sup> A. Abragam and M. H. L. Pryce, Proc. Roy. Soc. (London) **205A**, 135 (1951).

<sup>8</sup> R. E. Watson and A. J. Freeman, Phys. Rev. **123**, 2027 (1961).

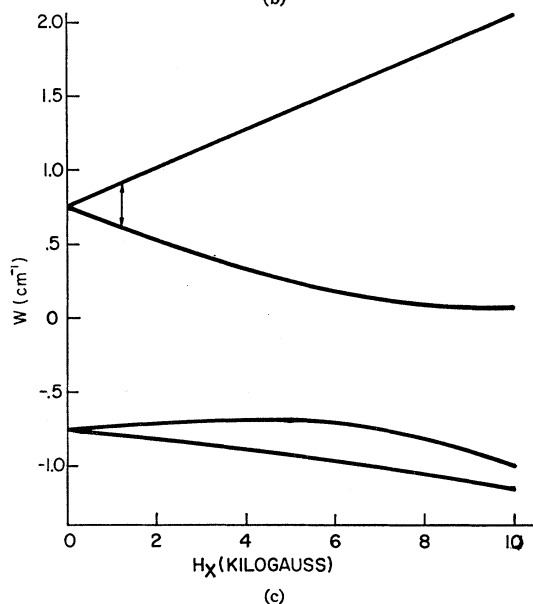
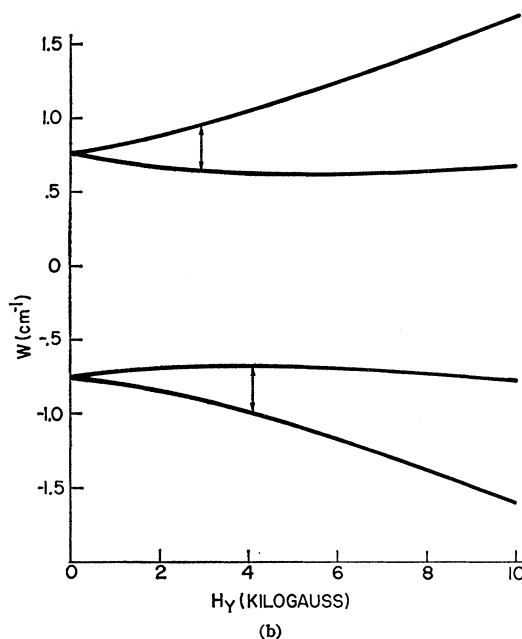
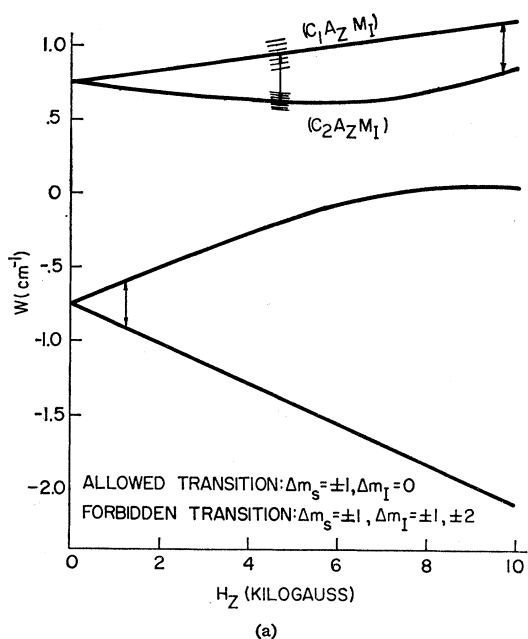


FIG. 6. Energy levels of Cr<sup>3+</sup> ion in substitutional sites versus dc magnetic field applied along the principal axes: (a)  $H_{dc} \parallel z$  axis, (b)  $H_{dc} \parallel y$  axis, and (c)  $H_{dc} \parallel x$  axis.

where

$$\left[ \frac{\partial W_i}{\partial H} \Big|_{H_0} - \frac{\partial W_j}{\partial H} \Big|_{H_0} \right] (\Delta H)_0 = m_I \Delta W_i - m_I \Delta W_j$$

$$= \left[ \frac{\partial W_i}{\partial H} \Big|_{H_0} - \frac{\partial W_j}{\partial H} \Big|_{H_0} \right] \frac{A_z m_I}{g\beta}. \quad (5)$$

Hence  $A_z m_I = g\beta(\Delta H)_0$ , provided  $|g\beta H_0| \gg |A|$  and  $(\partial W_i / \partial H)|_{H_0} - (\partial W_j / \partial H)|_{H_0} \neq 0$ . In other words, the additional magnetic field  $(\Delta H)_0$  between successive peaks due to hf (or shf) interaction is the same no matter whether the transition is within a predominantly  $\pm \frac{1}{2}$  doublet or a predominantly  $\pm \frac{3}{2}$  doublet.

The "forbidden transitions,"<sup>9,10</sup> i.e.,  $\Delta m_s = \pm 1$ ,  $\Delta m_I = \pm 1, \pm 2$ , may be allowed, if there exists a quadrupole interaction, a second order hfs (or shfs), or if there exists a component of rf magnetic field  $\parallel H_{dc}$ . The forbidden transitions  $\Delta m_I = \pm 1$  give peaks at

$$(\Delta H)_1 = \frac{\frac{\partial W_i}{\partial H} \Big|_{H_0} A_z m_I - \frac{\partial W_j}{\partial H} \Big|_{H_0} A_z (m_I \pm 1)}{g\beta \left[ \frac{\partial W_i}{\partial H} \Big|_{H_0} - \frac{\partial W_j}{\partial H} \Big|_{H_0} \right]}. \quad (6)$$

<sup>9</sup> W. Low, in *Solid State Physics*, Suppl. 2, edited by F. Seitz and D. Turnbull (Academic Press Inc., New York, 1960).

<sup>10</sup> J. E. Drumheller and R. S. Rubins, *Phys. Rev.* **133**, A1099 (1964).

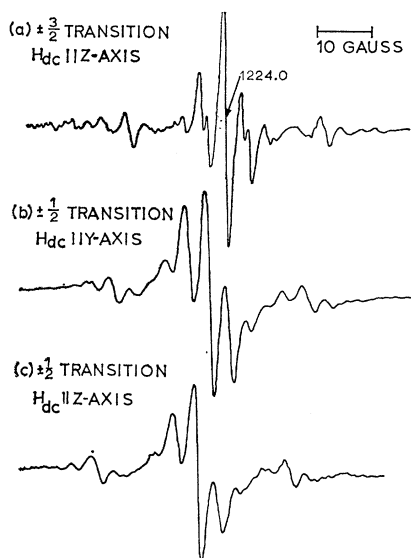


FIG. 7. Line shapes of the  $(\text{EPR})_I$  spectrum: (a)  $\pm\frac{3}{2}$  transition with  $H_{dc} \parallel z$  axis, (b)  $\pm\frac{1}{2}$  transition with  $H_{dc} \parallel y$  axis, and (c)  $\pm\frac{1}{2}$  transition with  $H_{dc} \parallel z$  axis.

The additional magnetic fields  $(\Delta H)_2$  required for observing  $\Delta m_I = \pm 2$  forbidden transitions are

$$(\Delta H)_2 = \frac{\left. \frac{\partial W_i}{\partial H} \right|_{H_0} A_z m_I - \left. \frac{\partial W_j}{\partial H} \right|_{H_0} A_z (m_I \pm 2)}{g\beta \left[ \left. \frac{\partial W_i}{\partial H} \right|_{H_0} - \left. \frac{\partial W_j}{\partial H} \right|_{H_0} \right]} \quad (7)$$

Since  $(\Delta H)_0$ ,  $(\Delta H)_1$ , and  $(\Delta H)_2$  are not equal in general, lines are broadened because of the superposition of peaks at different positions. However, if  $(\partial W_i / \partial H)|_{H_0} = -(\partial W_j / \partial H)|_{H_0}$  as in the case of a single electron Kramers doublet ( $S = \frac{1}{2}$ ), Eqs. (6)–(7) reduce to

$$(\Delta H)_1 = \frac{1}{g\beta} A_z (m_I \pm \frac{1}{2}) \quad (8)$$

and

$$(\Delta H)_2 = -\frac{1}{g\beta} A_z (m_I \pm 1). \quad (9)$$

The positions of successive peaks due to  $(\Delta H)_1$  and  $(\Delta H)_2$  coincide with those due to  $(\Delta H)_0$ , if  $m_I = \frac{1}{2}n$  (where  $n = \text{integer}$ ). The shf (or hf) interaction is well resolved provided  $|A| > \text{line width}$ . From Fig. 6(a), the lines of the predominantly  $\pm\frac{3}{2}$  transition must be narrower than that of the predominantly  $\pm\frac{1}{2}$  transition. Line shapes of  $\pm\frac{1}{2}$  and  $\pm\frac{3}{2}$  transitions at different  $H_{dc}$  orientations are shown in Fig. 7. These shapes remain unchanged even at 1.5°K, which confirms that they are shf broadened. Since lines due to shf interactions do overlap even at 1.5°K, nothing can be said about whether each individual line is a Gaussian or a Lorentzian.

TABLE I. Theoretical intensity ratios.

| $n \setminus \sum m_I$ | 0 | $\frac{1}{2}$ | 1      | $\frac{3}{2}$ | 2       |
|------------------------|---|---------------|--------|---------------|---------|
| 2                      | 1 | 0.192         | 0.0094 |               |         |
| 4                      | 1 | 0.3606        | 0.0517 | 0.00335       | 0.00008 |
| 6                      | 1 | 0.488         | 0.113  |               |         |
| 8                      | 1 | 0.599         | 0.186  | 0.033         | 0.0041  |
| 10                     | 1 | 0.674         | 0.256  |               |         |

The EPR spectra of  $V^{4+}$ ,  $Cr^{3+}$ , and  $Fe^{3+}$  in  $SnO_2$  are shown in Fig. 8. They have some similarities which may be characteristic of the shf interaction due to tin nuclei.  $V^{4+}$  in  $SnO_2$  was first measured by Tucker,<sup>1</sup> and has been discussed quite extensively by Kasai,<sup>11,12</sup> Kikuchi *et al.*,<sup>13</sup> and Chen *et al.*<sup>14</sup> The following discussions will follow Refs. 13 and 14 closely.

The intensity ratio is usually a powerful tool for studying the hf or shf interaction and the number of equivalent nuclei in the surrounding. Since  $Sn^{117}$  and  $Sn^{119}$  have equal spin ( $I = \frac{1}{2}$ ) and almost equal nuclear moments they may be considered as a single isotope.

Let  $a$  be the natural abundance of the isotopes having  $I = \frac{1}{2}$ ,

$$a = a(Sn^{117}) + a(Sn^{119}) = 16.35\%,$$

and  $n$  be the number of positionally equivalent nuclei. The total probability for which  $\sum m_I = m$  is

$$p_m = \sum_{k=|2m|}^n \frac{1}{2^k} c_l^k a^k (1-a)^{n-k} c_k^n, \quad (10)$$

where  $l = (k/2) + m = \text{the number of nuclei having } m_I = +\frac{1}{2}$ , only those values of  $k$  for which  $l = k/2 + m = a$  positive integer are used in the summation. The

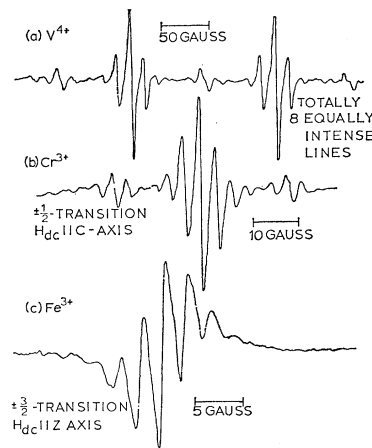


FIG. 8. EPR lines of  $V^{4+}$ ,  $Cr^{3+}$ , and  $Fe^{3+}$  in  $SnO_2$ : (a)  $V^{4+}$ , (b)  $Cr^{3+}$  ( $\pm\frac{1}{2}$  transition with  $H_{dc} \parallel c$  axis), and (c)  $Fe^{3+}$  ( $\pm\frac{3}{2}$  transition with  $H_{dc} \parallel z$  axis).

<sup>11</sup> P. H. Kasai, Phys. Letters 7, 5 (1963).

<sup>12</sup> Although the orbital splittings of  $V^{4+}$  in  $SnO_2$  have been predicted from the  $g$  anisotropies using crystal field theory, optical measurements failed to find any absorption in the region of  $6\mu$  to 5000 Å. The  $10Dq$  of  $V^{4+}$  in  $SnO_2$  is about 22 000  $cm^{-1}$ .

<sup>13</sup> C. Kikuchi, I. Chen, W. From, and P. Dorain, J. Chem. Phys. 42, 191 (1965).

<sup>14</sup> I. Chen, C. Kikuchi, and H. Watanabe, J. Chem. Phys. 42, 196 (1965).

TABLE II. Measured intensity ratios.<sup>a</sup>

|                  | $n \setminus \sum M_I$ |   |               |       |
|------------------|------------------------|---|---------------|-------|
|                  |                        | 0 | $\frac{1}{2}$ | 1     |
| $\text{V}^{4+}$  | "a" tins               | 1 | 0.205         |       |
|                  | "b" tins               | 1 | 0.396         | 0.053 |
| $\text{Cr}^{3+}$ | "a" tins               | 1 | 0.14          |       |
|                  | "b" tins               | 1 | 0.50          | 0.09  |
| $\text{Fe}^{3+}$ | "a" tins               |   | unresolved    |       |
|                  | "b" & "c" tins         | 1 | 0.62          | 0.204 |

<sup>a</sup> Error  $\pm 0.04$ .

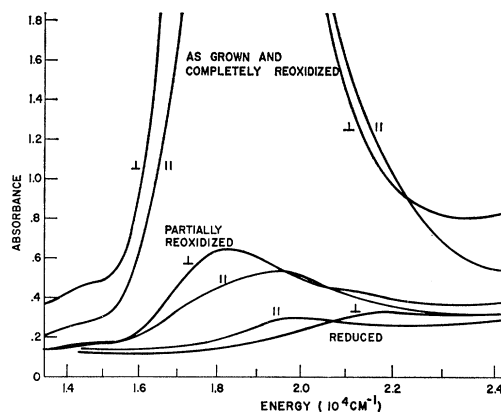
intensity ratios for different values of  $n$  are calculated as shown in Table I, where the ratios are normalized so that the intensity of the  $\sum m_I = 0$  line is always unity. According to Fig. 1, each substitutional site has three nonequivalent tin surroundings,<sup>13</sup> namely, (1) the "a" tin atoms—two nearest-neighbor tin atoms located along the  $c$  axis, (2) the "b" tin atoms—four nearest-neighbor tin atoms located in the  $xy$  plane, and (3) the "c" tin atoms—four nearest-neighbor tin atoms located in the  $xz$  plane. In the case of  $\text{V}^{4+}$ , the "a" tin atoms give the strongest shf interaction, because they are the closest in distance and have lobes of  $3d$  wave functions pointing toward them. The "c" tin atoms give the least shf interaction, because the  $3d$  wave function is zero when  $\theta = 0^\circ$ . Hence 2-tin and 4-tin patterns are expected in the  $\text{V}^{4+}$  case. However,  $\text{Fe}^{3+}$  is an "S-state" ion with an almost spherically symmetric orbital wave function. An equal contribution from "b" tin atoms and "c" tin atoms is expected. The measured intensity ratios are listed in Table II. The  $\text{V}^{4+}$  spectrum fits 2-tin and 4-tin patterns nicely. The  $\text{Fe}^{3+}$  spectrum fits better with 8- (or 10-) tin pattern. While the  $\text{Cr}^{3+}$  spectrum fits better with 2-tin and 6-tin patterns, which indicates that the contribution of "c" tin atoms is comparable with that of "b" tin atoms. The shf constants due to the "a" tin atoms diminish from  $\text{V}^{4+}$  to  $\text{Fe}^{3+}$ . The measured shf constants are listed in Table III.

$\text{Cr}^{53}$  has a nuclear spin  $I = \frac{3}{2}$  with a natural abundance of 9.54%. Four equally intense hf interaction lines should be expected. However, the intensity is only 2.4% of that of the main line ( $m_I = 0$ ), while the intensity of the shfs are  $\sim 20$ –50% of that of the main line ( $m_I = 0$ ). Thus the hf interaction may be masked by the strong shf interaction.

TABLE III. Spin Hamiltonian parameters of  $\text{Cr}^{3+}$  in  $\text{SnO}_2$ .<sup>a</sup>

|   | Substitutional site  | New lines (interstitial) |
|---|----------------------|--------------------------|
| $D$ ( $\text{cm}^{-1}$ )                              | $-0.6840 \pm 0.0002$ | $-0.7033 \pm 0.0002$     |
| $E$ ( $\text{cm}^{-1}$ )                              | $0.1852 \pm 0.0002$  | $0.1448 \pm 0.0002$      |
| $g_{av}$  | 1.975                | 1.975                    |
| $\Delta_0 = 2(D^2 + 3E^2)^{1/2}$ ( $\text{cm}^{-1}$ ) | $1.5108 \pm 0.0002$  | $1.4933 \pm 0.0002$      |
| $A_{Cr}$ (gauss)                                      | unresolved           | unresolved               |
| $({}^2A_{Sn})_i$ (gauss)                              | 37.4, 34.3, 35.1     | 40.1, 37.8, 36.7         |
| $({}^4A_{Sn})_i$ (gauss)                              | 7.0, 7.3, 7.0        | 8.9, 6.4, 9.1            |

<sup>a</sup> Where  $i = x, y, z$  and error =  $\pm 0.2$  G.

FIG. 9. Optical spectra of  $\text{Cr}^{3+}$ -doped  $\text{SnO}_2$  under various heat treatments.

### V. OPTICAL SPECTRA OF $\text{Cr}^{3+}$ IN $\text{SnO}_2$ SINGLE CRYSTAL

A  $\text{Cr}^{3+}$  ion has a  $(3d)^3$  electron configuration. Hund's rule determines the ground multiplet as  ${}^4F$ . The cubic crystalline field decomposes it into a singlet  ${}^4A_2$ , a triplet  ${}^4T_2$  and a triplet  ${}^4T_1$  of which  ${}^4A_2$  lies the lowest. The splitting of  ${}^4A_2$  and  ${}^4T_2$  is the so-called "10Dq" splitting, while the splitting between  ${}^4T_2$  and  ${}^4T_1$  is  $8Dq$ . The axial distortion leaves the orbital ground singlet a singlet ( $B_1$ ) but splits the orbital triplets into doublets ( $E$ ) and singlets ( $B_2, A_2$ ). Optical transitions corresponding to these energy levels are parity forbidden. However, weak optical absorptions are observed because of the state admixtures from the electron configuration of different parity. The dipole transition, which transforms like  $T_1$  in the  $O_h$  group, transforms like  $A_2$  and  $E$  in the  $D_{4h}$  group. Since  $E$  connects the ground singlet  $B_1$  and the excited doublet  $E$ , and  $A_2$  connects  $B_1$  and  $B_2$ , the  $\text{Cr}^{3+}$  optical absorption near 10Dq is expected to be dichroic.

The optical spectrum of  $\text{Cr}^{3+}$  in  $\text{SnO}_2$  is shown in Fig. 9. The as-grown crystal has strong absorption bands at  $19400 \text{ cm}^{-1}$  and  $18250 \text{ cm}^{-1}$  with light polarized parallel and perpendicular to the  $c$  axis, respectively. The band width is about  $3000 \text{ cm}^{-1}$ , and absorption coefficients are about  $100 \text{ cm}^{-1}$ . Measurements at  $20^\circ\text{K}$  showed these absorption bands to be slightly sharpened, with an additional weak band at  $14400 \text{ cm}^{-1}$  for light polarized perpendicular to the  $c$  axis. These absorption bands [designated (Opt)<sub>I</sub>] are much bigger than expected for  $\text{Cr}^{3+}$  transitions between  ${}^4A_2$  and  ${}^4T_2$ .<sup>15,16</sup> Other optical data in the infrared<sup>17</sup> and uv<sup>18,19</sup> regions correspond to the optical

<sup>15</sup> T. H. Maiman, R. H. Hoskins, I. J. D'Haenens, C. K. Asawa, and V. Evtuhov, Phys. Rev. **123**, 115 (1961).

<sup>16</sup> D. M. Dodd, D. L. Wood, and R. L. Barns, J. Appl. Phys. **35**, 1183 (1964).

<sup>17</sup> Robert Summitt and N. F. Borrelli, J. Phys. Chem. Solids **26**, 921 (1965).

<sup>18</sup> R. Summitt, J. A. Marley, and N. F. Borrelli, J. Phys. Chem. Solids **25**, 1465 (1964).

<sup>19</sup> S. F. Reddaway and D. A. Wright, Brit. J. Appl. Phys. **16**, 195 (1965).

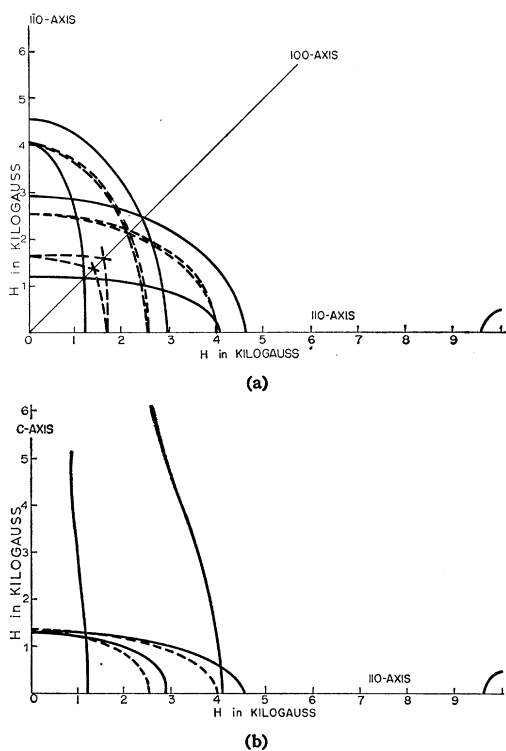


Fig. 10. The angular dependence of EPR spectra of a reduced  $\text{Cr}^{3+}$ -doped  $\text{SnO}_2$ : (a) on the  $c$  plane, and (b) on a plane containing the  $c$  axis and the  $[110]$  axis.

spectrum of the host  $\text{SnO}_2$  crystal. When the crystal is heat treated under a reducing atmosphere ( $\text{H}_2$  8%,  $\text{N}_2$  92%) at  $550^\circ\text{C}$  for 88 h, the strong  $(\text{Opt})_{\text{I}}$  absorption bands disappear completely. New weak bands appear at slightly different frequencies of  $21\,400\text{ cm}^{-1}$  and  $19\,700\text{ cm}^{-1}$  with light polarized perpendicular and parallel to the  $c$  axis, respectively. The absorption coefficients of these new bands [designated  $(\text{Opt})_{\text{II}}$ ] are approximately  $0.7\text{ cm}^{-1}$  (Table IV). Simultaneous with the change of  $(\text{Opt})_{\text{I}}$  to  $(\text{Opt})_{\text{II}}$  the characteristic absorption bands of the OH stretching vibration appear at  $3.07\ \mu$ ,<sup>20</sup> which indicates that hydrogen has diffused into the crystal.

When the crystal is heated in an oxygen atmosphere at  $800^\circ\text{C}$  for 72 h, the optical spectra revert to that observed in the as-grown crystal. As indicated in Fig. 9, as  $(\text{Opt})_{\text{I}}$  reappears it gradually obscures the  $(\text{Opt})_{\text{II}}$  spectrum while the absorption at  $3.07\ \mu$  simultaneously

TABLE IV. Optical Spectra of  $\text{Cr}^{3+}$  in  $\text{SnO}_2$ .

|                                   | As-grown crystal |                    | Reduced crystal |                    |
|-----------------------------------|------------------|--------------------|-----------------|--------------------|
|                                   | $\perp c$ axis   | $\parallel c$ axis | $\perp c$ axis  | $\parallel c$ axis |
| $h\nu$ ( $\text{cm}^{-1}$ )       | 18 250           | 19 400             | 21 400          | 19 700             |
| $h\Delta\nu$ ( $\text{cm}^{-1}$ ) | 3000             | 2700               | 700             | 800                |
| $\alpha$ ( $\text{cm}^{-1}$ )     | $\sim 100$       | $\sim 80$          | 0.5             | 0.7                |

<sup>20</sup> E. E. Kohnke, J. Phys. Chem. Solids **23**, 1557 (1962).

disappears, which indicates that hydrogen leaves the crystal lattice in the reoxidation process.

The optical spectra of  $\text{V}^{4+}$  and  $\text{Fe}^{3+}$  show no significant changes under either of these heat treatments.

## VI. THE EPR SPECTRUM OF $\text{Cr}^{3+}$ IN $\text{SnO}_2$ UNDER HEAT TREATMENTS

When  $\text{SnO}_2$  single crystals doped with  $\text{V}^{4+}$ ,  $\text{Cr}^{3+}$ , or  $\text{Fe}^{3+}$  are heat treated under a reducing atmosphere, a slight decrease in resistivity has been observed. The  $\text{Cr}^{3+}$  in  $\text{SnO}_2$ , which shows the dramatic change in optical spectrum mentioned above, has the following changes in EPR spectra. (1) The intensity of the EPR spectrum discussed in Sec. IV [designated  $(\text{EPR})_{\text{I}}$ ] for a reduced crystal decreases to only  $\frac{3}{4}$  of what it was originally in an as-grown crystal. (2) A new EPR spectrum [designated  $(\text{EPR})_{\text{II}}$ ] indicating four non-equivalent sites has been observed in the angular dependence as shown in Fig. 10. These spectra cross over at the  $[100]$  axis, the  $c$  axis, and the  $[110]$  axis with the  $z$  axes tilted  $\pm 0.5^\circ$  from the  $[110]$  axis. The line shapes of  $(\text{EPR})_{\text{II}}$  are shown in Fig. 11. The spin Hamiltonian of  $(\text{EPR})_{\text{II}}$  has the same expression as Eq. (1). The parameters of the spin Hamiltonian have been analyzed and are listed in Table III. From the argument given in Sec. II, there is a possibility that  $(\text{EPR})_{\text{II}}$  is due to  $\text{Cr}^{3+}$  ions in interstitial positions I, i.e.,  $(\pm a/2, 0, nc/2)$  and  $(0, \pm a/2, nc/2)$ .

When the crystal is reoxidized, the intensity of  $(\text{EPR})_{\text{II}}$  gradually vanishes, while the intensity of  $(\text{EPR})_{\text{I}}$  is regained gradually, and recovers completely after a thorough reoxidation.

## VII. DISCUSSIONS AND CONCLUSION

(1) The symmetry of the angular dependence of EPR spectra easily verifies that the  $\text{V}^{4+}$ ,  $\text{Cr}^{3+}$ , or  $\text{Fe}^{3+}$

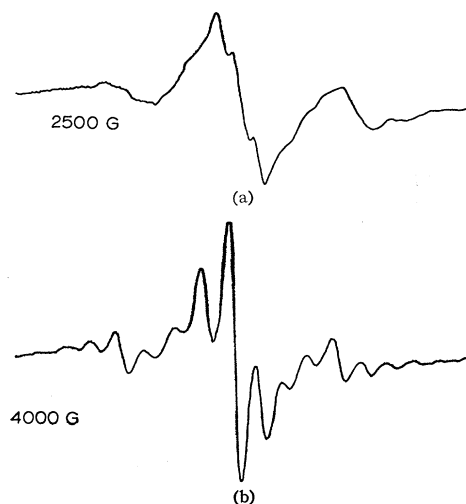


Fig. 11. Line shapes of the  $(\text{EPR})_{\text{II}}$  spectrum. (a)  $\pm\frac{1}{2}$  transition with  $H_{dc} \parallel y$  axis, (b)  $\pm\frac{1}{2}$  transition with  $H_{dc} \parallel z$  axis.

ion is usually located in a substitutional site in an as-grown  $\text{SnO}_2$  single crystal. The new  $(\text{EPR})_{\text{II}}$  spectrum in a reduced  $\text{Cr}^{3+}$ -doped  $\text{SnO}_2$  single crystal has a great similarity with the  $(\text{EPR})_{\text{I}}$  spectrum. The half-integer spin character indicates that  $(\text{EPR})_{\text{II}}$  must be due to  $\text{Cr}^{3+}$  ions, but in a different environment. One may suggest that the  $\text{OH}^-$  ion, formed after H atoms diffused into the crystal, replaces one of the oxygen ions on the tetragonal axis and causes the  $z$  axis to tilt slightly.<sup>21</sup> However, it is unlikely that such a relatively small change in the surroundings could explain a drastic decrease of the spin-Hamiltonian parameter  $E$  and an increase of the shf interaction constants.

The  $(\text{EPR})_{\text{II}}$  spectrum may be due to  $\text{Cr}^{3+}$  ions in the interstitial position I, which has four magnetically nonequivalent sites. The changes in the spin Hamiltonian parameters may then be explained as follows: The interstitial position I {i.e.,  $[\pm a/2, 0, (c/2)n]$  and  $[0, \pm a/2, (c/2)n]$ , where  $n$  is an integer} has a strong tetragonal distortion since the two oxygen ions along the tetragonal axis are very close (only 3.44 Å apart). When the  $\text{Cr}^{3+}$  ion moves into the interstitial position I, the distance between the two oxygen ions must be increased to about 4.1 Å apart which reduces the tetragonal distortion to about the same magnitude as the tetragonal distortion in the substitutional site. The rhombic distortion is caused mostly by the four oxygen ions in the  $xy$  plane. From Fig. 12 the four oxygen ions in interstitial position I are 2.343 Å apart from the central ion and make an angle of  $94.4^\circ$  instead of 2.051 Å and  $78.1^\circ$  as in the substitutional site; the rhombic distortion must be considerably reduced. The measured spin Hamiltonian parameters of the  $(\text{EPR})_{\text{II}}$  spectrum indeed indicate a slight increase in  $D$  and strong decrease in  $E$ . Furthermore, because the tin ions are relatively closer and have their tetragonal axis tilted, a stronger shf interaction with slightly higher anisotropy is expected.

The analyzed spin-Hamiltonian parameters as shown in Table III do reflect the phenomenological description. Hence we conclude that the  $(\text{EPR})_{\text{II}}$  spectrum is probably due to  $\text{Cr}^{3+}$  ions in the interstitial position I, in contrast with rutile in which interstitial impurities are usually in position II.<sup>22,23</sup> Why 25% of the  $\text{Cr}^{3+}$  ions can

<sup>21</sup> G. D. Watkins, Phys. Rev. **113**, 79 (1959).

<sup>22</sup> R. D. Shannon, J. Appl. Phys. **35**, 3414 (1964).

<sup>23</sup> H. B. Huntington and G. A. Sullivan, Phys. Rev. Letters **14**, 177 (1965).

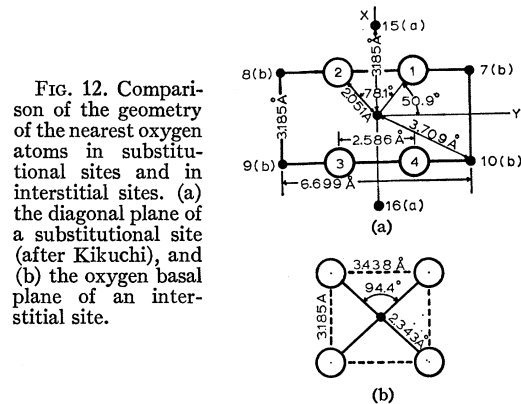


FIG. 12. Comparison of the geometry of the nearest oxygen atoms in substitutional sites and in interstitial sites. (a) the diagonal plane of a substitutional site (after Kikuchi), and (b) the oxygen basal plane of an interstitial site.

leap out of the substitutional site into the interstitial site in the presence of hydrogen atoms, and leap back in the reoxidation process, is still a question. Perhaps it is related to the thermal energy and the change of the energy barrier caused by the  $\text{OH}^-$  ion.

(2) There may be some correlation between the EPR spectra and the optical spectra. Both  $(\text{Opt})_{\text{I}}$  and  $(\text{Opt})_{\text{II}}$  spectra occur where the  $\text{Cr}^{3+}$  spectrum is supposed to be, and these spectra only exist in a  $\text{Cr}^{3+}$ -doped  $\text{SnO}_2$ . Thus the two optical spectra are likely due to  $\text{Cr}^{3+}$  ions in different environments. Because a reduced crystal still has 75% of  $\text{Cr}^{3+}$  in the substitutional sites (EPR data), while the optical spectrum has only the weak  $(\text{Opt})_{\text{II}}$  spectrum left, the  $(\text{Opt})_{\text{II}}$  spectrum must be due to  $\text{Cr}^{3+}$  ions in substitutional sites. Hence, the cubic-crystal field splitting  $10Dq$  is about  $20\,000\text{ cm}^{-1}$ , and the tetragonal distortion is about  $2000\text{ cm}^{-1}$ .

The intensity of the  $(\text{Opt})_{\text{I}}$  spectrum implies the existence of an appreciable opposite parity perturbation of the  $(3d)^3$  state of the  $\text{Cr}^{3+}$  ion. The nature of this perturbation is not yet known.

#### ACKNOWLEDGMENT

The authors would like to express their appreciation to J. A. Marley for his kindness in providing doped  $\text{SnO}_2$  single crystals, to Professor P. S. Pershan of Harvard University, J. W. H. Schreurs, and F. P. Koffyberg for helpful discussions, and to H. K. Rockstad for carefully reading the manuscript before publication. J. Tennant who helped measure the EPR spectra and T. A. Cook and H. L. Hoover who helped measure the optical spectra also are acknowledged with thanks.